Journal of Applied Electrochemistry (2005) 35:249–258
DOI 10.1007/s10800-004-6705-7

Improvement of a cementation process by ultrasound: case of the cadmium–zinc couple at a RDE

N.T. PHAM, M. AUROUSSEAU*, F. GROS and P. OZIL
Laboratoire d'Electrochimie et de Physico-chimie des Matériaux et des Interfaces, UMR 5631 CNRS-INPG-UJF, ENSEEG, BP 75, F-38402 St Martin d'Hères, France
*(*author for correspondence, Current address: Laboratoire de Génie des Procédés Papetiers, UMR 5518 CNRS-EFPG-INPG-CTP, BP 65, F-38402 St Martin d'Hères, France; e-mail: Marc.Aurousseau@efpg.inpg.fr)*

Received April 14 2004; accepted in revised form 4 November 2004

Key words: cadmium, cementation, kinetics, rotating disc electrode, 20 kHz ultrasound

Abstract

This paper describes the impact of low frequency (20 kHz) ultrasound (US) on Cd(II)/Zn cementation implemented on a RDE geometry. With and without US the reaction is mass-transfer controlled with two-step first-order kinetics mainly connected to deposit evolution. US improves the kinetics but to a lower extent than expected from electrochemical Cd(II) reduction. The favourable turbulence enhancement due to the deposit without US is not present when applying US because the deposit is continually removed from the surface. The influence of parameters such as temperature, initial concentration of reactants and US power is also analysed.

List of symbols

A	Geometrical electrode area (m^2)
C	Concentration of electroactive species (mol m^{-3})
C_0	Initial concentration of electroactive species (mol m^{-3})
D	Diffusion coefficient (m^2 s^{-1})
E_a	Apparent activation energy (J mol^{-1})
E_{cem}	Cementation potential (V/Hg–Hg_2SO_4)
E_{eq}	Equilibrium potential (V/Hg–Hg_2SO_4)
E_{rest}	Rest (open circuit) potential (V/Hg–Hg_2SO_4)
E^0	Standard equilibrium potential (V)
F	Faraday's constant (96486 C mol^{-1})
h_{e-US}	Distance (gap) between electrode and US probe (m)
i	Current density (A m^{-2})
i_{lim}	Limiting current density (A m^{-2})
K	Overall rate constant (s^{-1})
k	Mass transfer coefficient (m s^{-1})
m_c	Specific mass of produced metal at t_c (kg m^{-2})
n	Number of electrons involved
P_{US}	Ultrasonic power (W)
t	Time (s)
t_c	Critical or transition time (s)
T	Temperature (°C or K)

Greek symbols

ν	Kinematic viscosity (m^2 s^{-1})
ω	Rotation rate of the RDE (rad s^{-1})

Subscripts

0	Initial
1	First period (step) of the cementation run
2	Second period (step) of the cementation run
c	Critical or transition
Corrected	Corrected by volume variation throughout the run
Levich	Related to the Levich's equation from Relation (3)
US	Related to ultrasound
US theo.	Related to ultrasound from electrochemical ('theoretical') experiment

1. Introduction

Electrochemical cementation consists of a heterogeneous redox reaction occurring between metallic ions M^{m+} in solution and a more electropositive sacrificial solid metal S, generally leading to the deposit of metal M as follows:

$$s\,M^{m+} + m\,S \Leftrightarrow s\,M + m\,S^{s+} \quad (1)$$

Consequently, many processes have been developed for removing metals from solutions, generally using metal powders, in order either to recover precious metals or to avoid pollution by toxic metal ions. The main domains of application are hydrometallurgy [1–6], surface [7–9] and industrial waste [10–12] treatments and electrolyte purification [13–15]. For most systems [16–18], mass transfer of the noble metal ion controls the reaction rate and cementation kinetics can be modelled by an overall first-order reaction rate corresponding to diffusion–convection control. For example, recent works have highlighted the role of the evolution of the active surface area [19] or the deposit roughness [20]. The evolution of M^{m+} concentration, C (C_0 at t=0), within a batch stirred-tank reactor is described by:

$$\ln\left(\frac{C_0}{C}\right) = Kt = k\frac{A}{V}t, \quad (2)$$

where K is the overall rate constant, k the liquid–solid mass-transfer coefficient, V the volume of solution and

A the exchange area approximated by the geometrical electrode area.

Therefore, the use of ultrasound (US) during cementation is expected to improve efficiency, as observed in metal finishing [21], leaching [22] or other electrochemical reactions [23], through: (i) increased liquid–solid mass transfer; (ii) continuously regenerated and activated sacrificial metal surface; (iii) reduced agglomeration of metal particles.

The aim of this article is to investigate and quantify these effects on cementation kinetics with emphasis on the first two phenomena. It investigates the Cd(II)/Zn system, chosen due to the toxicity of cadmium, and uses a zinc rotating disc electrode (RDE) to ensure well-defined hydrodynamic conditions. The corresponding cementation reaction, i.e. Cd(II) + Zn ⇔ Cd + Zn(II), could reach thermodynamic completion, because of its high equilibrium constant value ($10^{12.2}$ at 25 °C [20]). Finally, low frequency US (20 kHz) was expected to favour the physical effects of acoustic cavitation and to limit other induced ultrasonic chemical effects in the solution.

2. Experimental details

Non-ultrasonic (silent) electrochemical and cementation experiments were carried out in a standard RDE measuring set consisting of a glass conical-bottomed vessel (60 mm internal diameter) with a water jacket ensuring temperature control and a capillary supplying ultrapure nitrogen (O_2 content below 5 molar ppm) to remove oxygen by bubbling for 30 min and blanketing the gas phase during experiments. The vessel could be equipped with a pH probe and three electrodes depending on the experiment: a 5 mm diameter working RDE (Tacussel EDI 101T device) made of cadmium or zinc (high purity >99.99%) and embedded into PTFE 11-mm rods, a saturated Hg/Hg_2SO_4 reference electrode (0.658 V/NHE at 25 °C) and a gold counter-electrode. The working electrode surface was carefully polished with diamond pastes of decreasing particle size down to 1 μm and washed for 5 min in ethylic alcohol under ultrasonic field. This procedure ensures excellent reproducibility of the electrode surface behaviour (standard deviation lower than 0.5% for electrochemical experiments and 5% for cementation experiments) and no additional electrochemical activation is required.

For ultrasonic experiments, the cell was the same except for a large hole in the conical-bottom made of PTFE to pass the horn in front of the RDE (Figure 1): identical results were found in the two cells for silent experiments. This was a standard titanium horn with a 35 mm diameter tip emitting 20 kHz US supplied from a 450 Sonifier model (Branson Ultrasonics Corporation, Great Britain). The ultrasonic power, P_{US}, provided to the solution by the electrical generator was assimilated to the thermal power determined by the standard calorimetric method [24]. Forty-four percent efficiency was obtained up to a 85 W electrical power without any volume or solution type influence in the range 100–200 cm^3 with distilled water or sodium sulphate medium. Moreover, the working electrode did not rotate during ultrasonic experiments.

All chemicals were of analytical grade (Normapur or Rectapur, Prolabo, France). The ionic strength of all solutions was adjusted at 1.0 M by adding sodium sulphate: migration phenomena and local variations of ionic strength were therefore neglected. Natural pH (ranging from 5.7 to 6) was maintained in this study and the side corrosion due to the action of acidic solutions remained negligible throughout the experiments with a

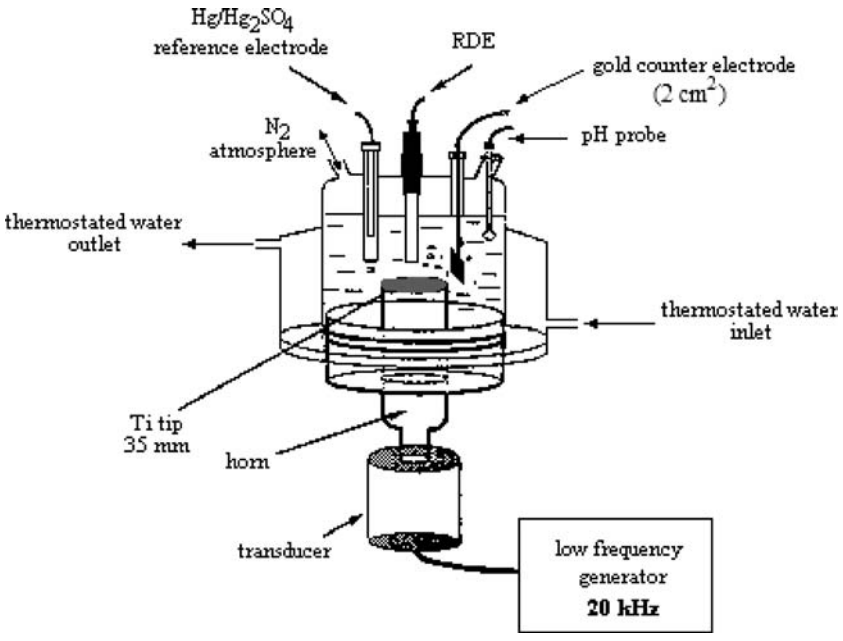

Fig. 1. Experimental set-up for ultrasonic experiments.

zinc consumption below 0.1%. Because of both the pH value and the concentration ranges, 0.89–17.8 mol m^{-3} for Cd(II) and 0–76.5 mol m^{-3} for Zn(II), these species were expected to be present in the solution mainly as $Cd(SO_4)_4^{6-}$ and $Zn(SO_4)_4^{6-}$. US induced no indirect chemical effects on Cd(II) and Zn(II) species as shown by unchanged concentrations after 2 h under US. The solution containing only 4.45 mol m^{-3} Cd(II) species in sulphate medium of unit ionic strength at 25 °C will henceforth be termed the 'standard' solution.

For cementation experiments, 1 cm^3 liquid samples were analysed at regular intervals by atomic absorption using a Varian AA-10 spectrophotometer: the resulting progressive decrease in solution volume, initially of 100 or 140 cm^3, was taken into account [20]. The surfaces of deposited metal were observed and analysed using a 6400 JEOL model for both scanning electronic microscopy (SEM) and energy dispersive spectroscopy (EDS).

3. Results and discussion

3.1. *Electrochemical study*

Voltamograms at steady-state, obtained with potential scanning at 10 mV s^{-1}, allowed us to determine the diffusion coefficient of Cd(II) and to construct Evans' diagrams to predict the limiting cementation reaction step. They were also used to choose optimal operating conditions for the reaction under US and to obtain theoretical mass-transfer coefficients for cementation with and without US.

3.1.1. *Diffusion coefficient of Cd (II)*

The silent cathodic polarisation curves (Figure 2, left) obtained for the reduction of Cd(II), in the concentration range 0.89–17.8 mol m^{-3}, on a Cd RDE, with a rotation speed ω varying from 30 to 315 rad s^{-1}, show a plateau corresponding to mass-transfer control by diffusion–convection of Cd(II). Levich's relationship for laminar flow:

$$i_{\lim} = -0.62\, D^{2/3}\, v^{-1/6} \omega^{1/2} n\, F\, C \qquad (3)$$

with the kinematic viscosity, v, measured by Ubbelohde technique at 9.9×10^{-7} m^2 s^{-1}, was used to estimate the Cd(II) diffusion coefficient D as 7.0×10^{-10} m^2 s^{-1} with a standard deviation of 2%, at 25 °C in a sulphate medium of 1 M ionic strength.

3.1.2. *Prediction of limiting step through Evans' diagrams*

Cementation can be considered as the combination of cathodic deposition and anodic dissolution. The limiting step can thus be determined by using techniques such as Evans' diagrams for corrosion reactions as proposed by Power and Ritchie [25] and recently used by Alemany et al. [20] or Jeffrey et al. [26]. Figure 2 shows diagrams obtained with and without US. The noise on the cathodic polarisation curve under ultrasonic field (Figure 2, right) results from the implosion of cavitation bubbles on the electrode surface. Nevertheless, after curve smoothing a plateau is clearly observed corresponding to a high value of the limiting current density.

In all cases the operating cementation point (E_{cem}; $i = 0$) is located on the Cd(II) diffusion plateau of the reduction wave with and without US. Thus, cementation is controlled by transport of Cd(II) species towards the zinc surface. Moreover, the predictive power of the Evans' diagrams is confirmed by comparing the predicted E_{cem} values to those measured at the beginning of the cementation reaction. Without US, these values are identical (−1.45 V for the example given) and closely agree with those provided by Bednorz and Gnot [27]. Under US, the measured E_{cem} values is smaller (−1.40 V compared to −1.33 V from Evans' diagram) and corresponds to more cathodic potentials, confirming the mass transport limitation.

Given occurring side reactions, it is interesting to compare the rest (open circuit) potential, E_{rest}, measured

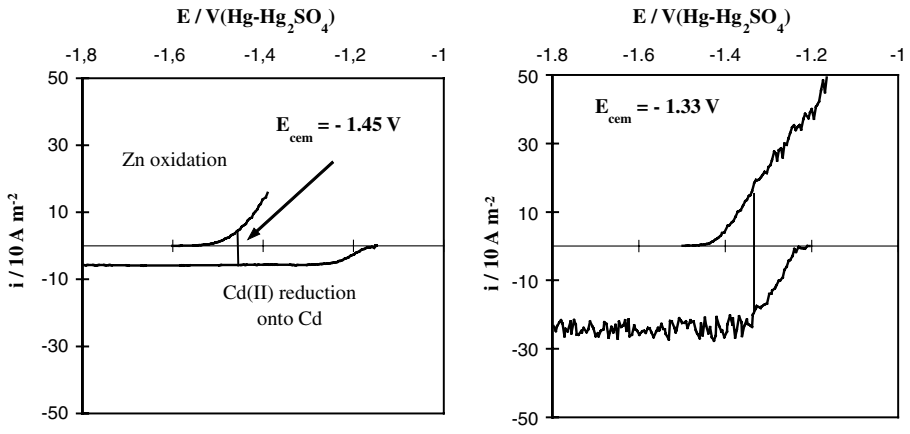

Fig. 2. Evans' diagrams for Cd(II)/Zn system with 'standard' solution −4.45 mol m^{-3} of Cd(II) and $T = 25$ °C and 'standard' conditions: $\omega = 157$ rad s^{-1} for silent experiment (left) and P_{US}=18 W for ultrasonic experiment (right).

for each polarisation curve and the equilibrium potential, E_{eq}, of the redox couple under study deduced from the Nernst equation:

$$E_{eq} = E^0 + \frac{RT}{nF} \ln\left(\frac{a(\text{ox})}{a(\text{red})}\right), \quad (4)$$

where a(ox) and a(red) are the respective activities assumed to be the molar concentrations in solution, i.e. 4.45×10^{-3} M for Cd(II) and 10^{-6} M for Zn(II) in the example given in Figure 2. This latter assumption is possible even for an ionic strength of unity due to the similar activity coefficients resulting from the similar speciation of both Cd(II) and Zn(II).

Without US, when the rest potential (−1.14 V) corresponds to the equilibrium (−1.13 V) for Cd(II) reduction, it is larger for Zn oxidation (−1.53 V compared to −1.6 V) due to the pH of 6. E_{rest} appears to be a mixed potential resulting from proton reduction to hydrogen evaluated at −1.01 V/Hg–Hg_2SO_4 from Relation (4). Under US, the observed differences are due to the presence of $OH^\bullet$ radicals produced by water sonolysis. For Cd(II) reduction, E_{rest} (−1.25 V) is lower than E_{eq} (−1.13 V) and corresponds to a lower interfacial Cd(II) concentration which could result from insoluble cadmium hydroxide formation on the electrode surface. For Zn oxidation, E_{rest} is still higher (−1.49 V compared to −1.53 V for E_{rest} without US and −1.6 V for E_{eq}) possibly due to an increase in Zn(II) concentration because of the chemical oxidation of Zn by $OH^\bullet$. For the electrochemical reduction of ions $[Fe(CN)_6]^{3-}$ under 20 kHz US, Compton et al. [28] also observed such potential displacement to more anodic potentials resulting from chemical re-oxidation of the electrogenerated ferrocyanide anion.

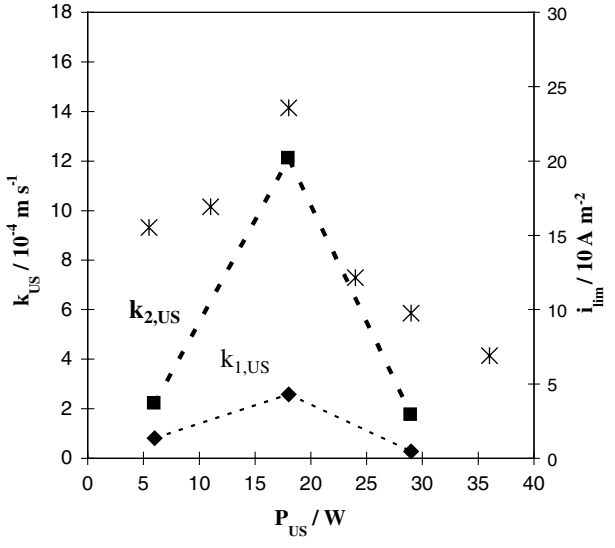

Fig. 3. Variation of the limiting current density of Cd(II) reduction on a Cd electrode (*, right scale) and mass-transfer coefficients ($k_{1,US}$ –♦– and $k_{2,US}$ –■–, left scale) during cementation versus ultrasonic power; 'standard' solution.

3.1.3. *Optimal working conditions for the reactor under US*

The evidence of the limitation by Cd(II) diffusion–convection, both with and without US, allowed the use of the limiting current density of species Cd(II) as a selection criterion for the optimal working conditions under US. The greater the limiting current density, i_{lim}, the greater the mass-transfer coefficient k and consequently the rate constant K of cementation reaction in the following equations:

$$i_{lim} = -k\ n\ F\ C \quad \text{with} \qquad k = K\frac{V}{A}. \quad (5)$$

Figure 3 (right scale) shows the evolution of i_{lim} vs. ultrasonic power, P_{US}, in the range 0–40 W. i_{lim} varies between 70 and 236 A m^{-2} with the maximum value obtained for approximately 18 W. At low powers, nucleation and growth of cavitation bubbles remain slow, leading to small bubbles that generate a weak implosion intensity and therefore limited turbulence close to the reaction surface. On the other hand, for high powers, the formation frequency and bubble size become large enough to create a gas layer near the ultrasonic probe that partially absorbs the ultrasonic waves and limits mass transfer [29]. Furthermore, the corresponding maximal specific ultrasonic power of 1.9 W cm^{-2} is very close to 2 W cm^{-2}, as determined by Negishi [30] from radiation strength measurements.

For an 18 W ultrasonic power, a 10^{-2} m electrode-horn gap and the 'standard' solution, no significant change was observed for i_{lim} when varying the solution volume, V, from 100 to 200 cm^3. Using luminol chemi-luminescence, Benahcene [31] showed that the intensity of the ultrasonic field is maximum close to the emission source at low frequencies and at the liquid surface at high frequencies. In our case, the zone located far from the ultrasonic probe may thus be considered as neutral and the volume variations as having no effect on the RDE surface reaction studied. Experiments were performed with a constant ultrasonic power of 18 W

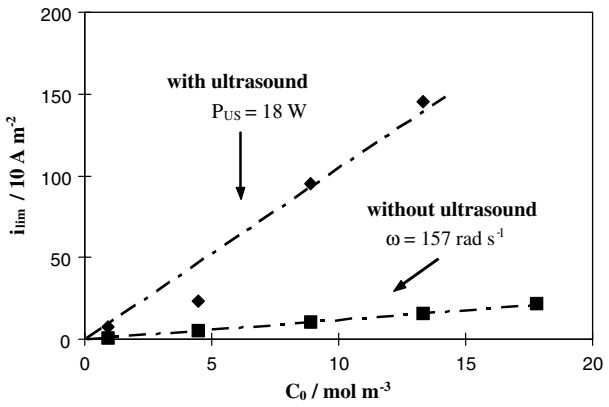

Fig. 4. Variation of the limiting current density of Cd(II) reduction on a Cd electrode versus Cd(II) species concentration with (–♦–) and without US (–■–); 'standard' solution and conditions.

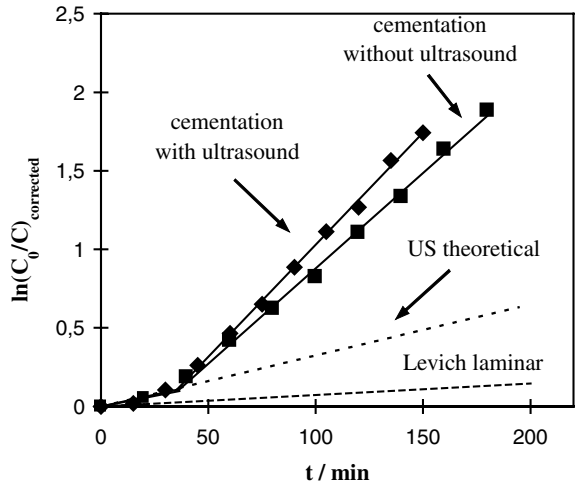

Fig. 5. Experimental and theoretical kinetic curves for cementation reaction of Cd(II) on Zn with (–♦–, $P_{US} = 18$ W) and without ultrasound (–■–, $\omega = 157$ rad s^{-1}); 'standard' solution and conditions.

and a volume of 200 cm^3 while varying the gap between the electrode and the ultrasonic probe, h_{e-US}, from 0.01 to 0.04 m. i_{lim} strongly decreased from 236 to 30 A m^{-2} as the gap increased. This result confirms that the ultrasonic field is maximal close to the ultrasonic probe at low frequency.

We can conclude, from the limiting current density of Cd(II) reduction, that the cementation under US should be optimal for $P_{US} = 18$ W, $h_{e-US} = 0.01$ m and solution volumes chosen at 100 or 140 cm^3 depending on the trials. Henceforth, these values shall be referred to as 'standard' US operating conditions.

3.1.4. *Expected mass-transfer coefficient for cementation reaction*

The expected positive effect of US on reaction kinetics can be quantified by comparing the mass-transfer coefficients deduced from the electrochemical experiments. Figure 4 shows how i_{lim} varies with and without US vs. Cd(II) concentration for trials performed in 'standard' solution and conditions. The slope of the resulting straight-line graphs provides the mass-transfer coefficients, k, from Equation (5). In the given example, working with US indicates that the k value increases from 6.21×10^{-5} to 5.41×10^{-4} m s^{-1}, i.e. a factor of 8.7. Using Equation (3) with the same D value as that without US, thus letting US only modify the boundary layer thickness from 11.3×10^{-6} to 1.3×10^{-6} m, it is possible to evaluate the equivalent rotation speed of a RDE leading to the k value obtained with US at 12 250 rad s^{-1}. This 'theoretical' value is consistent with other published values, typically ranging between 1300 and 40 000 rad s^{-1}, for such reactor configurations [23, 32].

The electrochemical study allows us to conclude that US at low frequency (20 kHz) does not modify the nature of the limiting step, in other words Cd(II) diffusion–convection, but dramatically improves mass transfer. At this stage, a similar enhancement could be expected on the cementation kinetics with a similar magnitude.

3.2. *Cementation kinetics*

3.2.1. *Kinetic curve characteristics*

For the same operating conditions as those of Figure 4, Figure 5 presents typical Cd(II)/Zn cementation kinetics as expressed in Equation (2), corrected for volume variation. Two 1st-order kinetic steps are observed, the second step being faster. This is the case both with and without US. The change in slope occurs at a similar

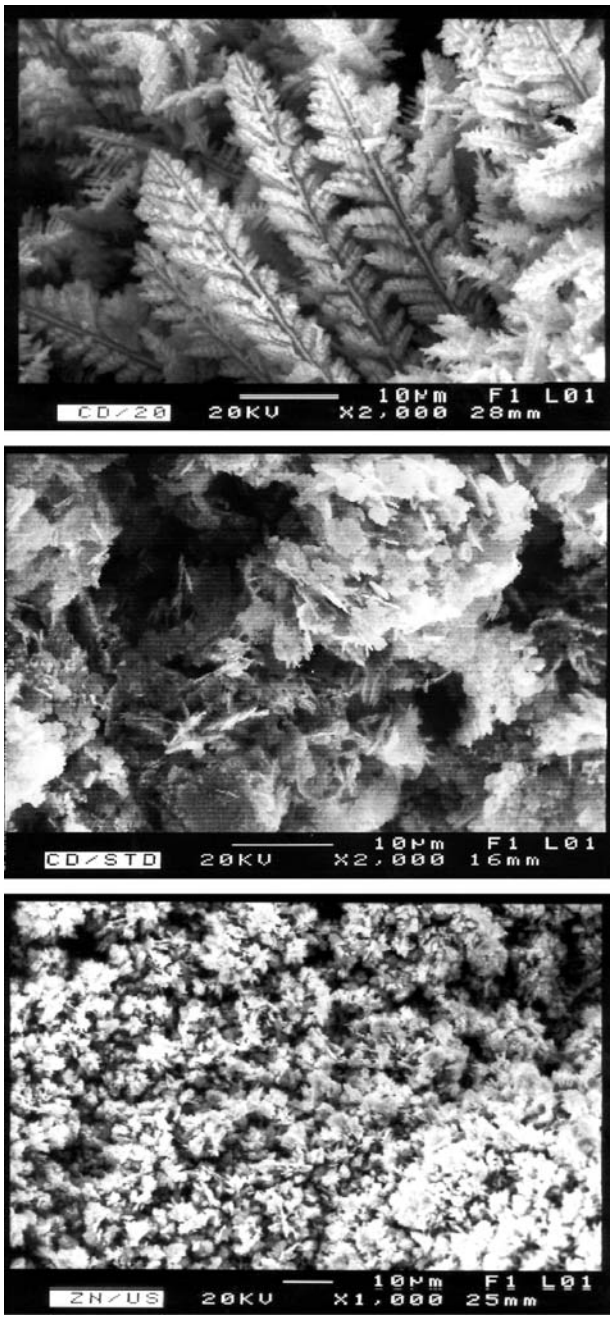

Fig. 6. SEM photographs of cadmium deposit obtained without ultrasound at ω=157 rad s^{-1} during the first kinetic step (top) and at reaction end (middle), and under US (bottom) for 'standard' solution and conditions.

Table 1. Experimental and theoretical mass-transfer coefficients with and without US for 'standard' solution and conditions

	$k_{theoretical}/10^{-4}$ m s^{-1}	$k/10^{-4}$ m s^{-1}	Comparison
Without ultrasound (ω = 157 rad s^{-1})	k_{Levich} = 0.621	k_1 = 2.27	k_1 = **3.65** k_{Levich}
		k_2 = 10.3	k_2 = **16.6** k_{Levich}
With ultrasound (P_{US} = 18 W)	$k_{US\ theo.}$ = 2.75	$k_{1,US}$ = 2.58	$k_{1,US}$ = **0.94** $k_{US\ theo.}$
		$k_{2,US}$ = 12.1	$k_{2,US}$ = **4.4** $k_{US\ theo.}$

Cd(II) conversion extent (respectively 10.3 and 9.2%) and within the 5–20% range typically observed [33–35]. In addition, this slope break occurs at the same critical time, t_c (35.6 ± 0.2 min), and the two curves are similar: the large increase in kinetics due to US expected from the electrochemical study is not confirmed. The deposit morphology is also different when applying US. For silent cementation, the Cd deposit is voluminous and remains fixed to the RDE throughout the trial (Figure 6). The initial dendritic structure observed during the initial stages of the reaction (Figure 6 top) changes with time to a facetted one (Figure 6 middle) due to a higher deposition rate. On the other hand, with US, the thin layer of deposit on the RDE (Figure 6 bottom) has a compact structure, meaning that the major part of the deposit is continuously removed as particles in suspension within the solution due to cavitation.

Table 1 presents the mass-transfer coefficients, deduced from the kinetic curves and Equation (2), for the two steps with US ($k_{1,US}$, $k_{2,US}$) and without US (k_1, k_2). They are compared with expected values, respectively k_{Levich} from Equation (3) and $k_{US\ theo}$. The real experimental value was chosen for reaction under US and not deduced from the straight line in Figure 4.

Without US, the first kinetic step is 3.65 times faster than expected from the Levich relationship. This is most convincingly explained by a change in hydrodynamics close to the reaction surface due to the formation of a large cadmium deposit early in the reaction. The increase in kinetics can be associated to a critical roughness, rather than simply to a critical deposited mass, m_c. This could induce a change in flow regime near the reaction surface, thus enhancing mass-transfer rate and altering the deposit morphology. The same observations were highlighted and quantified elsewhere [20] in terms of Reynolds and Sherwood numbers for zinc corrosion by species Ce(IV) or Cr(VI) due to micro-cavities inducing micro-turbulences.

With US, the first mass-transfer coefficient $k_{1,US}$ is very close to $k_{US\ theo}$. US enhances mass transfer on a plane surface since only a small amount of cadmium is deposited on the motionless RDE surface. Therefore, the increase in acceleration could also be attributed to the formation of a thin cadmium deposit leading to a change in local hydrodynamics. However, the global impact of ultrasound on kinetics is very weak. The US improvement factor, k_{US}/k, is close to unity for each kinetic step (1.15 instead of the expected 4.43), the acceleration factor, k_2/k_1, is similar (around 4.6) with and without US and the conversion extent is only slightly improved, from 77.5 to 82.5% after 150 min of cementation. This is due to two effects of acoustic cavitation, which are beneficial separately, cancelling each other out: the improvement of mass transfer and the regeneration of the reaction surface. The destruction of cadmium cement is thus negative with US in contrast to cementation without ultrasound.

The two kinetic curves obtained for 'standard' solution and conditions, a RDE rotating at 157 rad s^{-1} without US and fixed under a 18 W ultrasonic power were similar and these conditions shall be termed the 'reference' conditions. This allows a direct comparison of the variation observed with and without US.

3.2.2. *Influence of ultrasonic power*

Whereas for the RDE working without US, rotation is responsible for stirring, for the motionless RDE working with US, this role is undertaken by ultrasonic power, P_{US}. The aim of this part is to verify that the optimal working conditions with US correspond to those determined by the limiting current density for Cd(II) reduction.

Cementation kinetics were studied under 'standard' conditions for three ultrasonic powers: 6, 18 and 29 W. The corresponding mass-transfer coefficients are shown in Figure 3 (left scale). Despite the small number of experimental points (joined by straight lines for better reading), the optimum found in the electrochemical study was around 18 W and, because of cavitation, is clearly confirmed for the two kinetic steps. This result validates both kinetic control by mass transfer and the method used to determine the optimal conditions with US.

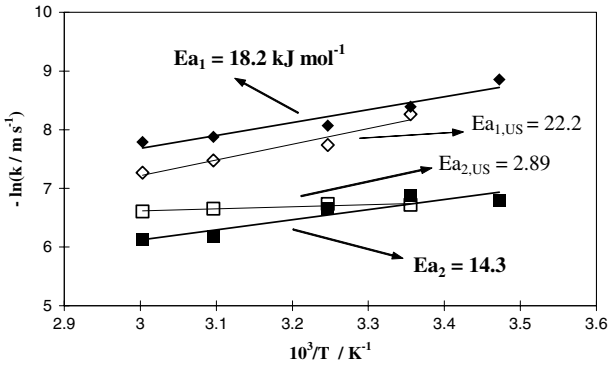

Fig. 7. Arrhenius plots for Cd(II)/Zn cementation experiments with and without ultrasound for 'standard' solution and conditions.

Table 2. Variation of mass-transfer coefficients and critical point characteristics vs. temperature for Cd(II)/Zn cementation reaction with and without US; 'standard' solution and conditions

T/°C	First step/10^{-4} m s^{-1}		Second step/10^{-4} m s^{-1}		Acceleration factor		Critical time/min		Critical deposit mass/10^{-1} kg m^{-2}	
	k_1	$k_{1,US}$	k_2	$k_{2,US}$	k_2/k_1	$k_{2,US}/k_{1,US}$	t_c	$t_{c,US}$	m_c	$m_{c,US}$
15	1.42	–	11.2	–	7.9	–	52.7	–	2.15	–
25	2.27	2.58	10.3	12.1	4.5	4.7	35.8	35.5	2.34	2.61
35	3.12	4.35	13.0	11.9	4.2	2.7	17.4	28.1	1.58	3.41
50	3.77	5.66	20.9	12.9	5.5	2.3	15.6	35.9	1.71	5.41
60	4.12	6.97	21.7	13.5	5.3	1.9	6.5	36.2	0.79	6.55

3.2.3. *Influence of temperature*

This parameter was studied in order to determine the apparent activation energy of reaction, E_a, and confirm the nature of the limiting step. Trials were performed in 'standard' conditions with and without US for temperatures ranging from 15 to 60 °C. However, a trial was not performed at 15 °C with US because the energy was too large to be dissipated within the solution.

Arrhenius plots of the mass-transfer coefficients versus T^{-1} presented on Figure 7 clearly show that the transfer rate increases with temperature both with and without US for the two kinetic steps. Resulting E_a values for both kinetic steps are consistent with a reaction controlled by mass transfer and agree with the accepted values of 16–17 kJ mol^{-1} for the Cd/Zn system without US [36, 37].

Other conclusions can be deduced from mass transfer coefficients and the characteristics of the critical (transition) point on kinetic curves (Table 2). Without US, the acceleration factor remains relatively constant with temperature, E_a values being very close for the two steps. k_1 increases with temperature while transition time decreases. This is due to faster appearance of the critical roughness leading to a change in hydrodynamics. m_c also decreases as temperature increases meaning that the deposit morphology changes with temperature during the first kinetic step and generates an increasing number of micro-turbulences.

Under US, the acceleration factor decreases with temperature mainly due to the weak evolution of $k_{2,US}$, leading to a much lower value for $Ea_{2,US}$ (Figure 7). The cadmium deposit is very thin and dense and corresponds to a limiting deposition rate under ultrasonic field. However, this reaction rate cannot be considered as an absolute limit because higher k_2 values may be obtained without US. t_c remains constant while $k_{1,US}$ increases by a factor of 2.7 within the temperature range under study, leading to a proportional increase in the amount of cadmium mass produced. In this case, it seems that the deposit structure induces fewer flow perturbations as temperature increases. Thus, a larger amount of produced deposit is required to reach the critical roughness.

Direct comparison of the values obtained shows that the global effect of US as temperature increases from 25 °C is to improve first step kinetics (a constant increase in $(k_{1,US}/k_1)_T$ up to 1.7) but to reduce second step kinetics (a decrease in $(k_{2,US}/k_2)_T$ down to 0.62). The resulting acceleration factors are lower with US and as temperature increases the reaction time to obtain high conversion extent (over 70%) also increases. US is therefore unfavourable for Cd(II)/Zn cementation reaction on RDE at high temperature (35–60 °C).

3.2.4. *Influence of initial Cd (II) concentration*

Experiments were performed in 'standard' conditions with and without US for several initial Cd(II) concentrations within the 0.89–17.8 mol m^{-3} range, i.e. approximately 100–2000 ppm mass. The ionic strength was maintained at 1 M by adding sodium sulphate to avoid any change in viscosity, migration, activity and diffusivity of species and resultant unexpected experimental variations.

Figure 8 shows the influence of initial Cd(II) concentration on mass-transfer coefficients and, consequently, on kinetic constants contrary to theory. A modification of first-order kinetics due to a variation of the initial Cd(II) concentration would thus modify the deposit morphology and the continuation of the reaction.

Without US, both the mass-transfer coefficients k_1 and k_2 present a maximum with a lower value for k_1 obtained for a higher initial Cd(II) concentration (respectively around 10 and 3–5 mol m^{-3}), in agreement with Lee et al. [37]. For the two higher concentrations,

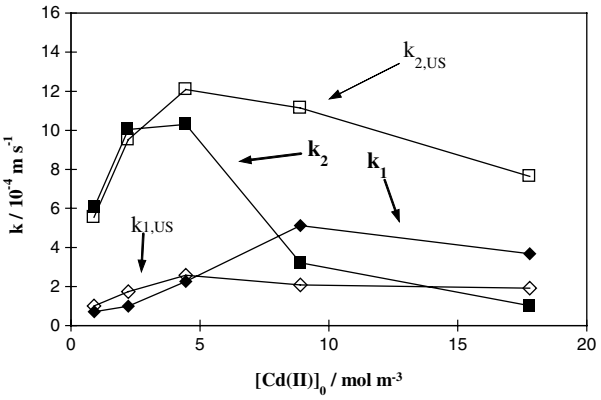

Fig. 8. Variation of mass-transfer coefficient vs. initial Cd(II) species concentration with ($k_{1,US}$ -◇- and $k_{2,US}$ -□-) and without ultrasound (k_1 -♦- and k_2 -■-) for 'standard' conditions.

Table 3. Variation of mass-transfer coefficients and critical point characteristics vs. initial Cd(II) species concentration for Cd(II)/Zn cementation reaction with and without US; 'standard' conditions

Initial Cd(II) concentration/mol m^{-3} $[Cd(II)]_0$	First step/10^{-4} m s^{-1}		Second step/10^{-4} m s^{-1}		Acceleration factor		Critical time/min		Critical deposit mass/10^{-1} kg m^{-2}	
	k_1	$k_{1,US}$	k_2	$k_{2,US}$	k_2/k_1	$k_{2,US}/k_{1,US}$	t_c	$t_{c,US}$	m_c	$m_{c,US}$
0.89	0.71	1.00	6.05	5.54	8.52	5.54	42.2	60.9	0.177	0.35
2.22	0.987	1.74	10.1	9.53	10.2	5.48	47.6	37.4	0.685	0.94
4.45	2.27	2.58	10.3	12.1	4.54	4.69	35.8	35.5	2.34	2.61
8.89	5.12	2.08	3.22	11.1	0.63	5.34	55.9	31.1	14.6	3.74
17.8	3.68	1.91	1.02	7.64	0.28	4.00	35.1	25.2	14.4	5.63

k_2 becomes lower than k_1, reflecting a reaction slowdown with acceleration factors lower than unity and decreasing with concentration (Table 3). SEM photos in Figure 9 show the faces of the cadmium deposit: internal face on the substrate side at reaction beginning and external face on the solution side at reaction end. Deposit morphology clearly changes from dendrites to compact granules (the thin needles were identified by EDS analysis as sodium sulphate and have no particular role *a priori*). The latter structure has a lower roughness that could be connected to the reaction slow down. In addition, the increases in reaction rate and k_1 with concentration should lead to a shorter transition time. In fact, no clear variation trend was observed and t_c remained constant. Increasing the deposition rate would decrease deposit roughness and therefore flow perturbation. This is confirmed in Figure 9 (top) where dendrites obtained during the first kinetic step for a Cd(II) concentration of 8.89 mol m^{-3} are both smaller and denser than those obtained for 4.45 mol m^{-3} (Figure 6, top). Moreover, the increase in m_c with Cd(II) initial concentration confirms the formation of a deposit inducing smaller flow perturbations (Table 3).

With US, t_c decreases as initial Cd(II) concentration increases. However, m_c increases simultaneously, meaning that the thin deposit has the same limited role on the flow as in the case without US. The acceleration factor remains constant, around the significant value of 5 (Table 3), showing a similar variation of the two mass-transfer coefficients so that the change in flow regime remains unmodified.

Finally, direct comparison of results obtained with and without US shows that the effect of US for increasing initial Cd(II) concentration is limited for concentrations lower than 4–5 mol m^{-3} (corresponding to $k_{1,US}/k_1)_{[Cd(II)]0}$ and $k_{2,US}/k_2)_{[Cd(II)]0}$ ratios from 0.92 to 1.76). For higher concentrations, this effect is negative for the first kinetic step, $k_{1,US}/k_1)_{[Cd(II)]0}$ about 0.5, but positive for the second step, $k_{2,US}/k_2)_{[Cd(II)]0}$ from 3.4 to 7.5. US results in a thin deposit layer instead of the globular layer which slows down kinetics which occurs without US. Applying ultrasound is thus favourable for cementation on RDE for high initial Cd(II) concentrations (5–18 mol m^{-3}).

3.2.5. *Influence of initial Zn(II) concentration*

Trials were performed in 'standard' conditions and constant ionic strength with and without US for several initial concentrations of species Zn(II), the oxidised form of the sacrificial metal within the range 0–76.5 mol m^{-3}, i.e. 0–5000 mass ppm.

Table 4 shows that the initial Zn(II) concentration barely influences cementation kinetics, both with and without US. This differs from the conclusions of Lee et al. [37] who worked at a very low initial ionic strength and observed a dramatic decrease in the kinetic rate as Zn(II) concentration increased. On the other hand, it

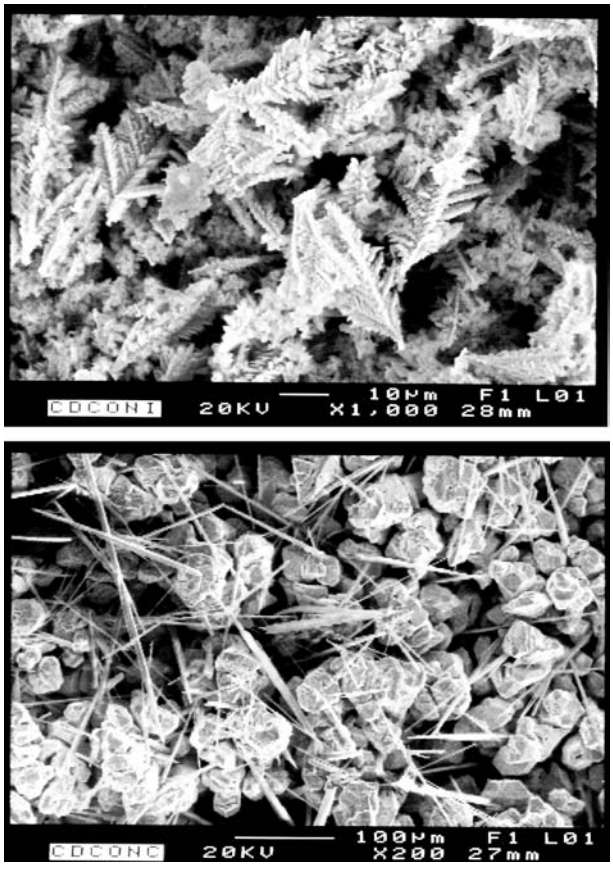

Fig. 9. SEM photographs of cadmium deposit obtained without ultrasound for a 8.89 mol m^{-3} initial Cd(II) species concentration at the beginning (top) and the end (bottom) of the cementation reaction; 'standard' conditions.

Table 4. Variation of mass-transfer coefficients and critical point characteristics Vs. initial Zn(II) species concentration for Cd(II)/Zn cementation reaction with and without US; 'standard' conditions

Initial Zn(II) concentration/mol m^{-3} $[Cd(II)]_0$	First step/10^{-4} m s^{-1}		Second step/10^{-4} m s^{-1}		Acceleration factor		Critical time/min		Critical deposit mass/10^{-1} kg m^{-2}	
	k_1	$k_{1,US}$	k_2	$k_{2,US}$	k_2/k_1	$k_{2,US}/k_{1,US}$	t_c	$t_{c,US}$	m_c	$m_{c,US}$
0.0	2.27	2.58	10.3	12.1	4.54	4.69	35.8	35.5	2.34	2.61
15.3	1.73	1.90	8.91	11.2	5.15	5.90	28.1	35.1	1.41	1.92
76.5	0.645	2.09	8.69	11.4	13.5	5.45	30.5	34	0.58	2.04

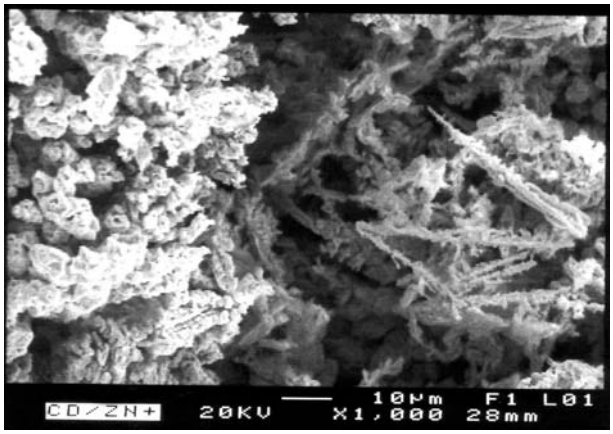

Fig. 10. SEM photograph of cadmium deposit obtained without US for a 15.3 mol m^{-3} initial Zn(II) species concentration at the end of the cementation reaction; 'standard' solution and conditions.

agrees with the work of Miller and Beckstead [38] for the Cu(II)/Zn system in similar conditions.

Without US, the acceleration factor increases with Zn(II) concentration mainly due to k_1 decrease. As concentration increases, the acceleration occurs for similar (occasionally slightly lower) transition times, although for a decreasing critical deposit mass. As a consequence, the resulting deposit has a greater ability to perturb the flow. Such influence of deposit morphology is confirmed on Figure 10 by SEM observations at reaction end showing that a poorly defined dusty deposit replaces the facetted structure.

With US, no significant effect of Zn(II) concentration is observed for mass transfer coefficients, transition time and critical deposit mass.

Direct comparison of results obtained with and without US shows that the impact of ultrasound remains limited as the initial Zn(II) concentration is increased. In fact most $k_{1,US}/k_1)_{[Zn(II)]0}$ and $k_{2,US}/k_2)_{[Zn(II)]0}$ ratios range between 1.1 and 1.3 and the characteristics of the transition point are very close both with and without US. The benefit of US is only significant for the highest concentration, i.e. 76.5 mol m^{-3}.

4. Conclusion

The cementation reaction of cadmium by zinc was studied both on a RDE without US and on the same motionless electrode under US at low frequency (20 kHz).

The electrochemical behaviour of the Cd(II)/Zn system was studied under controlled hydrodynamics. Cd(II) diffusivity was estimated at 7×10^{-10} m^2 s^{-1} in sulphate medium with an ionic strength of unity. Diffusion–convection transport of Cd(II) species to the reaction surface appeared to limit the cementation reaction from Evans' diagrams. Using US did not modify the nature of this limiting step but greatly enhanced mass transfer.

The main part of this work was the investigation of the kinetics of the Cd(II)/Zn cementation reaction. The previous limiting step was confirmed by two successive 1st-order kinetics characterised by apparent activation energies lower than 25 kJ mol^{-1} and by evidence of the influence of stirring intensity (by RDE rotation [20] or applying US). A change in hydrodynamics occurred implying an acceleration of the cementation reaction from a transition point characterised by a critical roughness. The emergence of this key factor related to critical mass and morphology quality depends on temperature and initial Cd(II) and Zn(II) concentrations.

The overall benefit of low frequency US on cementation kinetics is very limited, especially in comparison with the performance expected from the electrochemical study: e.g. for the 'reference' experiment, an improvement factor of 1.2 was obtained instead of the expected 4.5. The two effects induced by ultrasonic cavitation, increased mass transfer and regeneration of the reaction surface, act antagonistically: the latter is unfavourable for cementation because it leads to the destruction of the cadmium deposit which enhances cementation kinetics without US. Finally, cementation under ultrasonic field will only be improved at room temperature (lower than 30 °C) and for high initial Cd(II) concentrations of 5–18 mol m^{-3}. Nevertheless, for other processes, such as cementation on powder, the use of US should show other advantages, as presented elsewhere [39].

Acknowledgements

We are very grateful to Pr. C. Pétrier (LCME, Le Bourget du Lac, France) for the use of ultrasonic material and insight on ultrasound topics.

References

1. M.E. Wadsworth and J.D. Miller, Hydrometallurgical processes, *in* 'Rate Processes of Extractive Metallurgy' (Plenum Press, New-York, 1979), pp. 33–244.
2. J.D. Miller, R.Y. Wan and J.R. Parga, *Hydrometallurgy* **24** (1990) 373.
3. R. Gana, M. Figueroa, L. Kattan, D. Grandoso and M.A. Esteso, *J. Appl. Electrochem.* **29** (1999) 1475.
4. D. Stanojevic, B. Nikolic and M. Todorovic, *Hydrometallurgy* **54** (2000) 151.
5. S.H. Castro and M. Sanchez, *J. Cleaner Prod.* **11** (2003) 207.
6. Y. Kayanuma, T.H. Okabe, Y. Mitsuda and M. Maeda, *J. Alloy. Comp.* **365** (2004) 211.
7. S. Hirsch and C. Rosenstein, *Metal Finishing* (*63rd Guidebook and Directory Issue*) **93**(1A) (1995) 415.
8. T. Stefanowicz, M. Osinska and S. Napieralska-Zagozda, *Hydrometallurgy* **47** (1997) 69.
9. T.N. Vorobyova, S.K. Poznyak, A.A. Rimskaya and O.N. Vrublevskaya, *Surface Coat. Tech.* **176** (2004) 327.
10. M.T.A. Reis and J.M.R. Carvalho, *Minerals Eng.* **7**(10) (1994) 1301.
11. P.E. Charpentier, *Ph.D. Thesis*, INPG, Grenoble, France (1997).
12. S.A. Nosier and S.A. Sallam, *Sep. Purif. Technol.* **18** (2000) 93.
13. F. De Blander and R. Winand, *Electrochim. Acta* **20** (1975) 839.
14. K. Stole-Hansen, D.A. Wregget, D. Gowanlock and P.E. Thwa-ites, *Comput. Chem. Eng.* **21** (1997) S1099.
15. B.S. Boyanov, V.V. Konareva and N.K. Kolev, *Hydrometallurgy* **73** (2004) 163.
16. J.D. Miller, *Miner. Sci. Eng.* **5**(3) (1973) 242.
17. M. Fouletier, J.B. Matthieu and P. Noual, 'Les applications de l'électrochimie à l'hydrométallurgie' (Pluralis edition, Paris, 1980), chap. IX, pp. 129.
18. G.P. Power and I.M. Ritchie, Metal displacement reactions, in B.E. Conway and J.O. Bockris (Eds.), 'Modern Aspects of Electrochemistry' No. 11, Chap. 5 (Plenum Press, New York 1975) pp. 199–250.
19. C. Alemany, J.-P. Diard, B. Le Gorrec and C. Montella, *Electrochim. Acta* **41** (1996) 1483.
20. C. Alemany, M. Aurousseau, F. Lapicque and P. Ozil, *J. Appl. Electrochem.* **32** (2002) 1269.
21. R. Walker, *Adv. Sonochem.* **3** (1995) 125.
22. K.M. Swamy and K.L. Narayana, *Ultrason. Sonochem.* **8** (2001) 341.
23. D.J. Walton and S.S. Phull, *Adv. Sonochem.* **4** (1996) 205.
24. T.J. Mason, J.P. Lorimer and D.M. Bates, *Ultrasonics* **30** (1992) 40.
25. G.P. Power and I.M. Ritchie, *Aust. J. Chem.* **29** (1976) 699.
26. M. Jeffrey, S. Robertson, H. Zhang and E. Ho, 'Electrochemistry: the key to understanding hydrometallurgical reactions', Proceedings of the International Symposium honoring Prof. I.M. Ritchie, Vol. 2, Vancouver, Canada, 24–27 August (2003) pp. 1125–1140.
27. J. Bednorz and W. Gnot, *Pol. J. Chem.* **68** (1994) 1199.
28. R.G. Compton and J.C. Eklund, S.D. Page, *J. Phys. Chem.* **99** (1995) 4211.
29. D. Ensminger, 'Ultrasonics: Fundamentals, Technology, Applications', 2nd ed. revised and expanded (M. Dekker Inc., New York, 1988).
30. K. Negishi, *J. Phys. Soc. Jpn.* **16** (1961) 1450.
31. A. Benahcene, *Ph.D. Thesis*, University of Savoy, Chambéry, France (1994).
32. A. Benahcene, C. Petrier, G. Reverdy and P. Labbe, *New J. Chem.* **19** (1995) 989.
33. F. Lawson, Cementation kinetics, *in* M. Mohan Rao, K.P. Abraham, G.N.K. Iyengar and R.M. Mallya (Eds.), Thermodynamics and Kinetics of Metallurgical Processes (ICMS-81) (The Indian Institute of Metals, Calcutta, 1985), pp. 207–225.
34. T. Angelidis, K. Fytianos and G. Vasilikiotis, *Resour. Conserv. Recycl.* **2** (1989) 131.
35. G. Puvvada and T. Tran, *Hydrometallurgy* **37** (1995) 193.
36. T.R. Ingraham and R. Kerby, *Trans. Metall. Soc. AIME* **245** (1969) 17.
37. E.C. Lee, F. Lawson and K.N. Han, *Inst. Min. Metall.* **84** (1975) C87.
38. J.D. Miller and L.W. Beckstead, *Metall. Trans.* **4** (1973) 1967.
39. M. Aurousseau, N.T. Pham and P. Ozil, *Ultrason. Sonochem.* **11** (2004) 23.